Applied Catalysis B: Environmental 252 (2019) 41–46

Contents lists available at ScienceDirect

Applied Catalysis B: Environmental

journal homepage: www.elsevier.com/locate/apcatb

Strong effect of multi-electron oxygen reduction reaction on photocatalysis through the promotion of interfacial charge transfer

Jiajie Xu, Yanfeng Chen, Zhiyong Dong, Yanni Peng, Yue Situ, Hong Huang*

School of Chemistry and Chemical Engineering, South China University of Technology, Guangzhou 510640, PR China

ARTICLE INFO

Keywords:
TiO_2
ORR
Conjugated microporous polymers
Photocatalysis
IFCT

ABSTRACT

An efficient visible-light-driven photocatalyst with interface charge transfer (IFCT) effect was achieved by assembling Fe-porphyrin based conjugated microporous polymer on TiO_2 microspheres. It was revealed that IFCT effect played a crucial role in the enhancement of photocatalytic performance. In addition, the oxygen reduction reaction (ORR) activity of TiO_2 was enhanced in the presence of Fe-porphyrin based conjugated microporous polymer and IFCT effect was promoted obviously due to the high ORR activity. It's speculated that multi-electron ORR could accelerate the consumption of photoinduced electrons, retarding the recombination of photoinduced holes and electrons in the IFCT process, leaving more high-oxidizing photoinduced holes in the valance band of TiO_2 for further degradation. What's more, to further clarify the relationship between multi-electron ORR and IFCT effect, the influence of electron transfer number on the generation of photoinduced holes in the IFCT process was studied, and it was believable that four-electron oxygen reduction process was better able to accelerate the generation of photoinduced holes in the IFCT process than two-electron oxygen reduction process, resulting in higher photocatalytic activity.

1. Introduction

Semiconductor-based photocatalysis has been considered as one of the most important technologies for organic pollutant degradation and hydrogen production. Although wide-band gap semiconductors, such as TiO_2, ZnO and $SrTiO_3$, are considered as efficient photocatalysts owing to the high redox potential of photogenerated charge carries, they could only be excited under UV irradiation [1,2]. Heterogeneous photocatalysis with wide-band gap semiconductors presents a promising approach for efficiently utilizing solar energy, owing to much higher quantum efficiency compared to pristine semiconductors [3–5]. Some mechanisms for heterogeneous visible-light-induced photocatalysis, such as Z-scheme photocatalysis [6] and IFCT effect [7], have been proposed as further design guides for photocatalysts with high solar energy conversion.

IFCT effect has been demonstrated to be an efficient way for enhancing the separation of photoinduced electron–holes. Recently, Hashimoto group successfully constructed a series of visible-light-driven photocatalysts by grafting Cu (II) or Fe (III) cluster on the surface of wide-band gap semiconductors [8–10]. In these systems, photoinduced IFCT effect from semiconductors to the grafted clusters resulted in not only the extension of the photo response from UV to visible light region, but also the efficient consumption of photoinduced electrons via the reduction reaction of the grafted metallic clusters, simultaneously taking advantage of the high-oxidizing holes in the valance band for complete degradation of organic compounds [11]. Although electron reduction reaction of oxygen, during which the excited electrons were consumed, was found in the IFCT process, the quantum efficiency was still limited due to the weak charge separation.

In photocatalytic degradation, the oxidation of pollutants is significantly accelerated as strongly oxidizing species, such as H_2O_2 and $^{\cdot}O_2^-$, could be generated due to the reduction of molecular oxygen by photogenerated electrons [12–16]. Hence, it seems likely that ORR plays an important role in photocatalytic degradation. It has been reported that many microporous materials, such as metal-organic frameworks (MOFs) [17], covalent organic frameworks (COFs) [18] and conjugated microporous polymers (CMPs) [19], showed excellent ORR activity with high electron transfer number (n). Meyer et al. [20] have reported the synthesis of heme-functionalized TiO_2 compound, where multi-electron transfer was found from hemes to TiO_2 to accelerate the reductive process. As such, introducing high ORR activity to IFCT system might retard the recombination of photoinduced electron-holes, improving the quantum efficiency of the IFCT system.

Herein, Fe-porphyrin (denoted as FeP) and porphyrin based CMPs were assembled on the surface of TiO_2 microspheres (denoted as TiO_2-FeCMP and TiO_2-CMP) to prepare an efficient visible-light-driven

* Corresponding author.
E-mail address: cehhuang@scut.edu.cn (H. Huang).

https://doi.org/10.1016/j.apcatb.2019.03.075
Received 12 December 2018; Received in revised form 22 March 2019; Accepted 28 March 2019
Available online 31 March 2019

photocatalyst with IFCT effect, where multi-electron ORR was found to play a vital role in the promotion of IFCT effect. It's revealed that multi-electron ORR could accelerate the consumption of photoinduced electrons in the IFCT process, where more photoinduced holes in the valance band of TiO_2 were left for further degradation. What's more, the relationship between n value and the generation of photoinduced holes in the IFCT process was clarified, and it was believable that four-electron oxygen reduction process was better able to accelerate the generation of photoinduced holes in the IFCT process than two-electron oxygen reduction process, resulting in higher photocatalytic activity.

2. Experimental

2.1. Preparation

Preparation of 5, 10, 15, 20-tetrakis (4'-bromophenyl) porphyrin (Por). Porphyrin was prepared according to the procedure reported previously [19]. *P*-bromobenzaldehyde (5.58 g, 30 mmol) was added into the mixture of nitrobenzene (150 mL) and acetic acid (225 mL), and heated up to 120 °C, then, freshly distilled pyrrole (2.1 mL) was added and kept for 1 h. After cooling to room temperature, the as-prepared precipitate was collected by filtration and washed with methanol for several times. The product was further purified by recrystallization from chloroform and methanol twice.

Preparation of 5, 10, 15, 20-tetrakis (4'-bromophenyl) porphyrin Ferric (FeP) [21]. The as-prepared porphyrin (1.00 g) and $FeCl_3$ (869.2 mg) were placed in a 100 mL round-bottom flask and dried at 100 °C in vacuum overnight. Degassed DMF was added in the flask and stirred at 100 °C for 10 h. After cooling to room temperature, deionized water (200 mL) was poured into the mixture and the resulted product was filtered and washed with water and methanol. The crude product was further purified by recrystallization from chloroform and methanol twice.

Preparation of TiO_2-FeCMP compound. 1,5-cyclooctadiene (445 μL), bis (1,5-cyclooctadiene) nickel (0) (1.00 g) and 2,2'-bipyridyl (564.7 mg) were added into dehydrate dioxane (60 mL), and the mixture was kept at 100 °C for 1 h under argon atomosphere. Then, the as-prepared FeP (741.2 mg, see details in Supporting Information) was added into the mixture and stirred for 12 h before TiO_2 microsphere (2.80 g, see details in Supporting Information) was added to react for another 12 h. After cooling to the room temperature, concentrated HCl (20 mL) was dropped into the mixture, and the resulted precipitate was collected by filtration and washed with aqueous saturated EDTA solution, deionized water, $CHCl_3$ and THF, respectively. The crude product was further extracted by Soxhlet with methanol, acetone, and THF for 1 day, respectively, and dried at 100 °C under vacuum. The as-prepared product was denoted as TiO_2-FeCMP. The TiO_2-CMP was synthesized based on the as-prepared porphyrin (See details in Supporting Information) instead of FeP.

2.2. Characterization

X-ray diffraction (XRD) patterns of these samples were obtained in the range of 5-80° (2θ) using a Bruker D8 ADVANCE diffractometer (Cu Kα radiation, $\lambda = 1.54178$ Å). The morphologies were recorded by scanning electron microscopy (SEM, LEO 1530 V P) and transmission electron microscopy (TEM, Thermo Fisher Scientific, Tecnai-G20, 200 kV, USA). Fourier transform-infrared spectra (FT-IR) were recorded by infrared spectrometer (Bruker, Vector 33). UV–vis diffuse reflectance spectra were performed in a Hitachi Corporation UV-3010 spectrophotometer, using $BaSO_4$ as the reflectance standard. Nitrogen adsorption-desorption isotherms were obtained from an isothermal nitrogen sorption analyzer (TriStar 3010, Micromeritics USA). Surface chemical compositions and chemical status of the as-prepared samples were analyzed by X-ray photoelectron spectroscopy (XPS, K-Alpha, Thermo Fisher Scientific, USA). Electron spin resonance (ESR) spectra were conducted on a JEOL JES FA200 spectrometer.

2.3. Photocatalytic performance

The degradation of methyl orange (MO) solution (10 mg L^{-1}) was carried out to evaluate the photocatalytic performance of as-prepared samples under visible light irradiation. 30 mg of catalyst sample was mixed with 30 mL of methyl orange solution in a water-cool reactor. Prior to the irradiation under a PLS-SXE300 Xe lamp (Beijing Perfectlight Technology Co., Ltd) equipped with cutoff filters (420 nm, 475 nm and 530 nm), the suspension was stirred magnetically for 30 min in a dark box to reach an adsorption-desorption equilibrium. About 3 mL aliquots were taken and then filtered with a microspore membrane at a certain time interval. The Shimadzu UV-2050 spectrophotometer was used to record the maximum absorbance of the filtrate (462 nm for MO).

2.4. Electrochemical characterization

Electrochemical measurements of cyclic voltammetry, rotating disk electrode (RDE) were performed by a computer-controlled potentiostat (CHI 660, CH Instrument, China) with a three-electrode cell system, in which a glass carbon RDE (ATA-1B, Jiangfen Electroanalytical Instrument) after loading the electrocatalysts was used as the working electrode, an Ag/AgCl (KCl, 3 M) electrode as the reference electrode, and a Pt wire as the counter electrode. The electrochemical experiments were conducted in O_2 saturated 0.1 M KOH electrolyte for the oxygen reduction reaction. The potential range is cyclically scanned between −0.6 and 0 V in 0.1 M KOH at a scan rate of 100 mV s^{-1} at room temperature after purging O_2 or Ar gas for 15 min. RDE measurements were carried out at differe˙nt rotating speeds from 400 to 2500 rpm (see details in Supporting Information).

3. Results and discussion

The typical absorptions of porphyrin were found in the UV–vis diffuse reflectance spectra (Fig. 1). Compared to pure TiO_2 (Fig. 1a), TiO_2-FeCMP (Fig. 1c) and TiO_2-CMP (Fig.1d) showed typical B-band (ca. 420 nm) and Q-band (between 500 nm and 700 nm) of porphyrin, which suggested that porphyrin units were introduced into the compound successfully [22,23]. What's more, TiO_2-FeCMP only had one Q-band absorption while TiO_2-CMP had two absorptions, which might be ascribed to the good symmetry due to the insert of Fe ion [24]. A broad absorption of Fe-TiO_2 (Fig. 1b) between 450 nm and 500 nm was observed which revealed that Fe ion was grafted on the TiO_2 successfully [25]. The XRD patterns of the obtained samples (Fig. S1) were in good

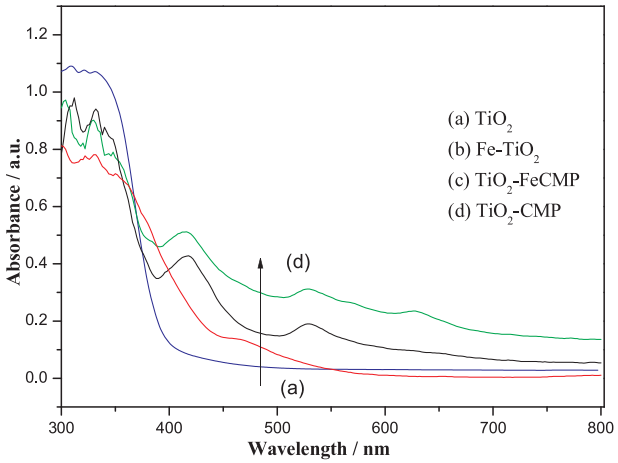

Fig. 1. UV–vis diffuse reflectance spectra.

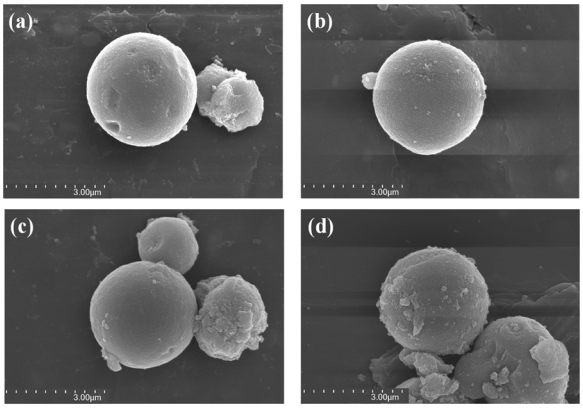

Fig. 2. SEM of (a) TiO_2, (b) Fe-TiO_2, (c) TiO_2-FeCMP and (d) TiO_2-CMP.

agreement with anatase TiO_2 (PDF card No. 21-1272) and no other obvious peaks were found with the CMP added. The Fourier transform infrared (FT-IR) spectrum (Fig. S2) of TiO_2-FeCMP revealed the absence of the characteristic C-Br vibration band at 1072 cm^{-1}, which illustrated that the FeP were covalently integrated into the compound [19]. Thermo gravimetric (TG) analysis (Fig. S3) showed that the content of CMP in the compound was up to 10.19%. EDX analysis indicated the presence of Ti, O, C, N and Fe (Fig. S4), and the content of Fe was up to 0.15%. These results demonstrated the successful fabrication of the TiO_2-FeCMP compound.

The morphology of the as-prepared samples were recorded by scanning electron microscopy (SEM). The SEM images (Figs. 2 and S5) revealed that pure TiO_2 microspheres (Fig. 2a) were in the range of 2–5 μm, and the incorporation of CMP made no difference on the morphology. To gain the insight into the morphology, transmission electron microscopy (TEM) was performed. As shown in Fig. 3, TiO_2-FeCMP possessed a highly mesoporous framework comprised of densely nanoparticles, and the STEM-mappings (Fig. S4a) clearly demonstrated the core-shell structure of the TiO_2-FeCMP. Nitrogen sorption analysis (Fig. 3d) revealed that pure TiO_2 microspheres had well mesoporous structure with Brunauer-Emmett-Teller (BET) surface area of ~219.4 $m^2 g^{-1}$. Although TiO_2 microspheres were encapsulated by CMP in TiO_2-CMP compound, well mesoporous structures were found in both TiO_2-FeCMP and TiO_2-CMP with BET surface area of ~231.0 and 212.5 $m^2 g^{-1}$ respectively. Well-defined mesoporous structure with a size of 3.86 nm was obtained for TiO_2-FeCMP (4.24 and 4.84 nm for TiO_2-CMP and TiO_2 respectively), which confirmed the well mesoporous structure of the CMP (Fig. 3e).

X-ray photoelectron spectroscopy (XPS) analysis revealed the presence of Ti2p, O1s, N1s, C1s and Fe2p in the compound (Figs. 4 and S6). The high-resolution N1s (Fig. 4a) spectra of TiO_2-FeCMP could be fitted to three different signals that corresponded to pyridinic N and Fe-N bonding (399.48 eV, N1), pyrrolic N (400.98 eV, N2) and graphitic N (401.88 eV, N3), respectively [26,27]. The high-resolution Ti2p (Fig. 4b) showed a doublet at 458.28 eV for $Ti2p_{3/2}$ and at 464.08 eV for $Ti2p_{1/2}$. In general, it's about 5.8 eV for the binding energy difference of $Ti2p_{3/2}$ and $Ti2p_{1/2}$, which is ascribed to the +4 oxidation state of Ti in TiO_2 [28]. However, Ti^{3+}2p could not be found remarkably, which indicated that there was no Ti^{3+} existed in the compound.

In order to evaluate the photocatalytic performance, MO was chosen as the main pollutant to degrade under visible light irradiation (Fig. 5a). TiO_2 showed no response to the visible light, while Fe-TiO_2 did, which was ascribed to IFCT effect from the valence band of TiO_2 to the surface Fe (III) clusters (Fig. S7a). The concentration of MO were reduced by about 47.6% and 94.9% for TiO_2-CMP and TiO_2-FeCMP, respectively. Moreover, TiO_2-FeCMP also showed the highest photocatalytic activity on phenol degradation (Fig. S7b). To clarify the IFCT process, the degradation of MO over TiO_2-CMP and TiO_2-FeCMP was carried out under different cut-offs (UV, visible light, > 475 nm and > 530 nm). As shown in Fig. 5b, there was no obvious difference in the MO removal under UV light for both TiO_2-CMP and TiO_2-FeCMP, as

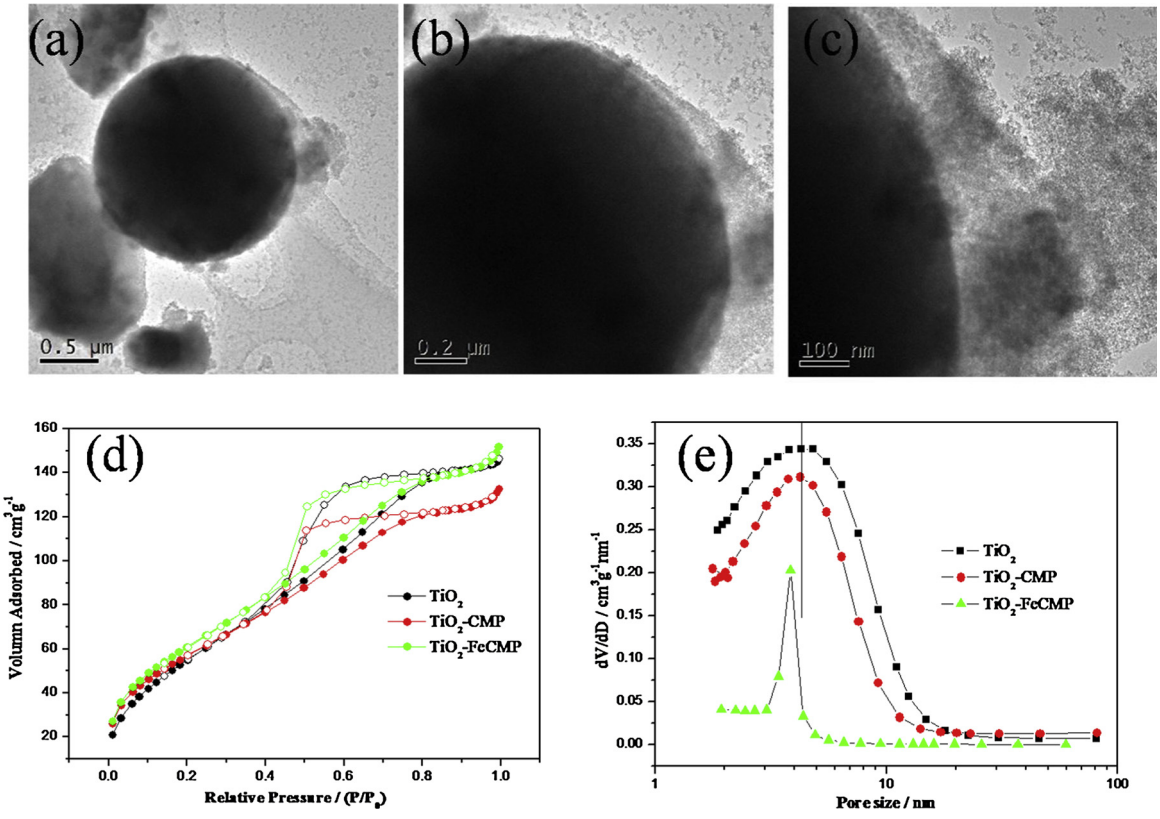

Fig. 3. (a) TEM of TiO_2-FeCMP, (b), (c) close inspection of TiO_2-FeCMP, (d) nitrogen sorption, (e) pore size distribution.

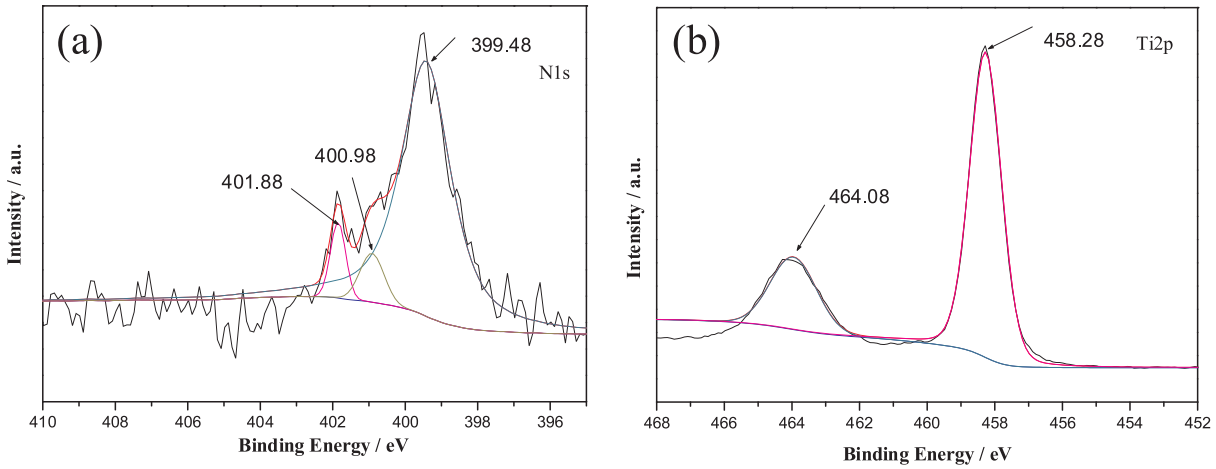

Fig. 4. XPS spectra of TiO_2-FeCMP, (a) N1s, (b) Ti2p.

the both holes in the valence band could be excited under UV light. As for visible light and λ > 475 nm, the MO removal fell inconspicuously for TiO_2-FeCMP, while for λ > 530 nm, the removal dropped sharply from 82.2% to 12.6%, which confirmed the IFCT effect in the TiO_2-FeCMP compound. It was speculated that IFCT was triggered by assembling FeP based conjugated microporous polymers on TiO_2 microspheres.

To further confirm IFCT process in the TiO_2-FeCMP, the DMPO-$^{\cdot}CH_2OH$ spin adducts formed in the visible light irradiated methanol and 5,5-dimethyl-1-pyrroline-*N*-oxide (DMPO) suspensions of TiO_2-FeCMP and TiO_2-CMP in the absence of oxygen were recorded by ESR measurements [11] (Fig. 6, see details in Text S7). In the case of TiO_2-FeCMP (Fig. 6a), the characteristic ESR sextet peaks of the DMPO-$^{\cdot}CH_2OH$ spin adducts were found, and the intensities of sextet peaks increased under visible light irradiation. As for TiO_2-CMP (Fig. 6b), no ESR signals were observed even under visible light irradiation. This indicated that the photoinduced holes in the valance band of TiO_2 could be effectively generated over TiO_2-FeCMP under visible light irradiation. It was obvious that IFCT effect could be triggered from the valance band of TiO_2 to the Fe (III) in the FeCMP. Furthermore, compared with Fe-TiO_2 (Fig. S7c), much more photoinduced holes could be generated, which demonstrated the importance of CMP structure.

Moreover, it was revealed from the trapping experiments (Fig. S8) that $^{\cdot}OH$, h^+ and $^{\cdot}O_2^-$ had different influence on the degradation results and h^+ was the most critical species. It seemed feasible that IFCT process was supposed to be the main reason for the higher photocatalytic activity of TiO_2-FeCMP, while the photocatalytic activity of TiO_2-CMP was ascribed for the $^{\cdot}O_2^-$. However, the MO removal of TiO_2-FeCMP under argon ambient (Fig. S9) dropped from 94.9% to 26.6%, which suggested that O_2 behavior might be bound up with IFCT effect. It was speculated that multi-electron ORR might promote the IFCT process, resulting in higher photocatalytic activity.

In order to investigate the relationship between ORR and IFCT process, TiO_2-FeCMP with different reaction time were prepared (Text S9), which were denoted as TiO_2-FeCMP0, TiO_2-FeCMP6 and TiO_2-FeCMP18 (Fig. S10, Supporting information). Moreover, electrochemical measurements were employed to gain further insight into the photocatalytic mechanism. Cyclic voltammetry (CV) in N_2 and O_2 saturated 0.1 M KOH was employed to examine the ORR catalytic activity of TiO_2-FeCMP series at a scan rate of 100 mV s^{-1} (Figs. 7a and S12). In the N_2 saturated solution, a featureless slope for the cathodic current was presented for all of the CV curves within the entire potential range. Whereas, a well-defined cathodic current peak was found at all of the CV curves in the O_2 saturated electrolyte, suggesting a prominent ORR activity for TiO_2-FeCMP series. Moreover, rotating-disk electrode (RDE) measurements in 0.1 M KOH saturated with O_2 were performed on TiO_2-FeCMP series (Figs. 7b and S13). According to the Koutecky-Levich equation (See Supporting Information for detail), the electron transfer number (n) of TiO_2-FeCMP was calculated to be 3.32 at 0.45 to 0.5 V vs. RHE (Fig. 8), suggesting a mainly four-electron oxygen reduction process. And for TiO_2-FeCMP6, the n value was calculated to be 2.39, containing both two-electron oxygen reduction process and four-electron oxygen reduction process (Fig. S15b). In contrast, TiO_2-FeCMP0 and TiO_2-FeCMP18 exhibited much lower n values of 1.83 and 2.07, which were ascribed to a two-electron oxygen reduction process

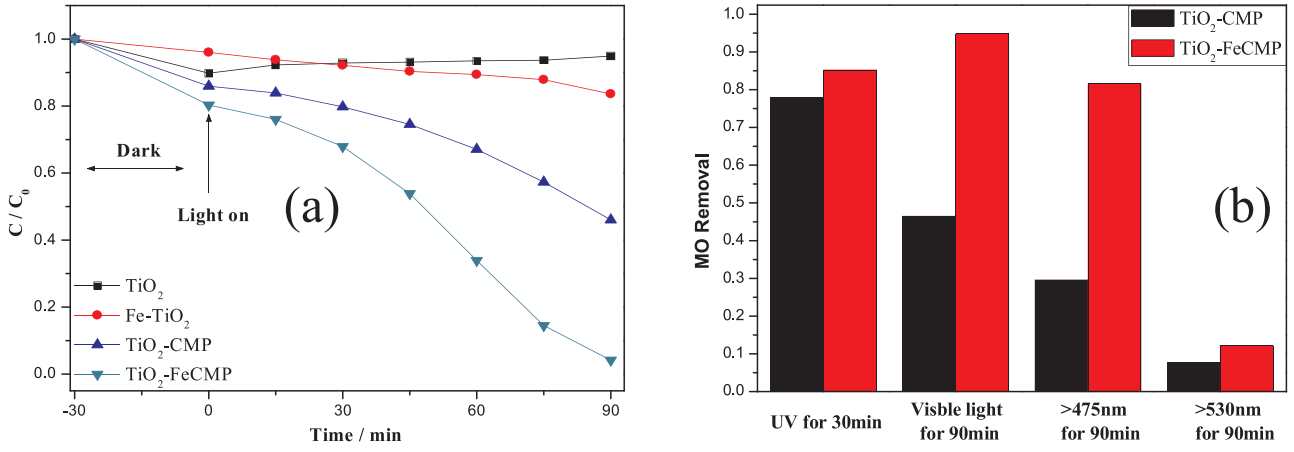

Fig. 5. (a) Photocatalytic degradation curves of MO, (b) photocatalytic degradation under different cut-offs.

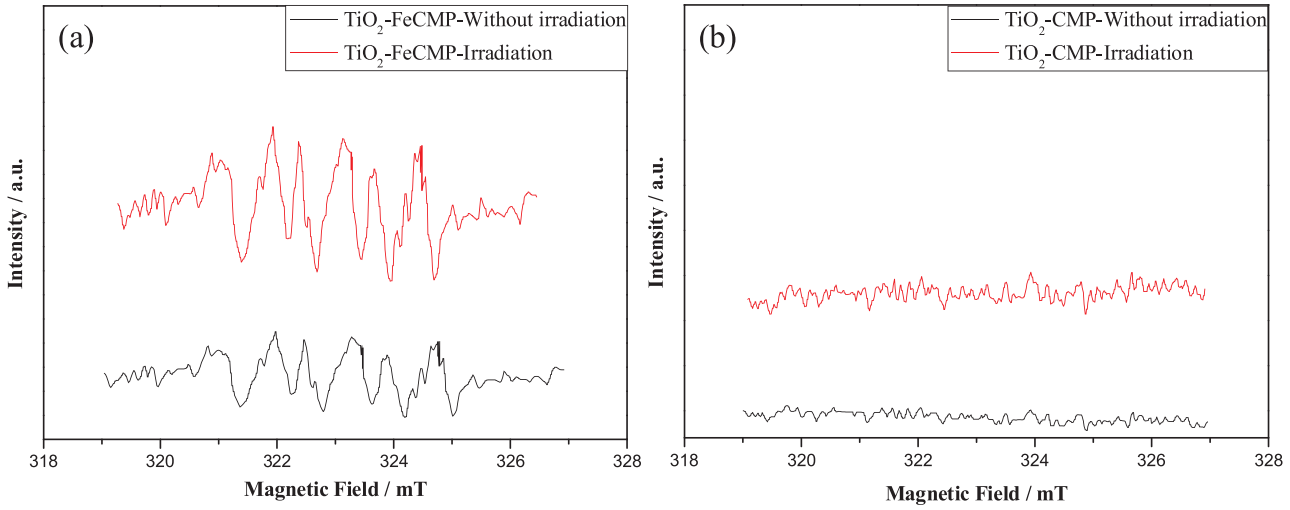

Fig. 6. ESR spectra of (a) TiO_2-FeCMP, (b) TiO_2-CMP.

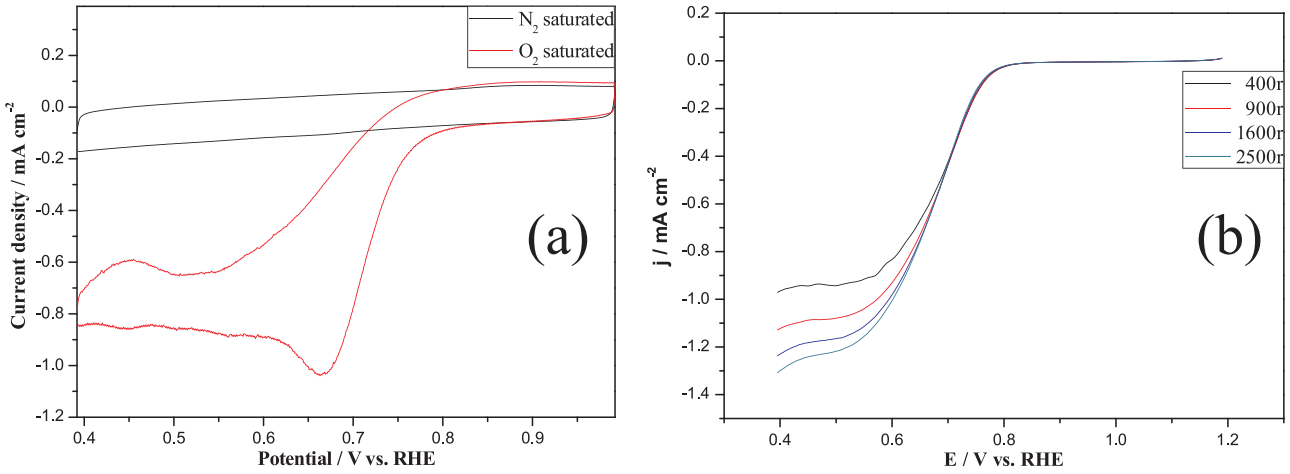

Fig. 7. (a) Cyclic voltammetry of TiO_2-FeCMP, (b) LSV curves of TiO_2-FeCMP at different rotation rates in O_2-saturated 0.1 M KOH.

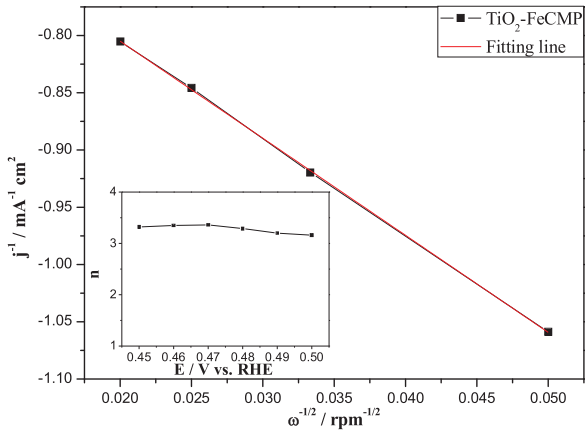

Fig. 8. Koutecky-Levich plots of TiO_2-FeCMP at 0.45 V, the inset sows the dependence of electron transfer numbers (n) at different electrode potentials.

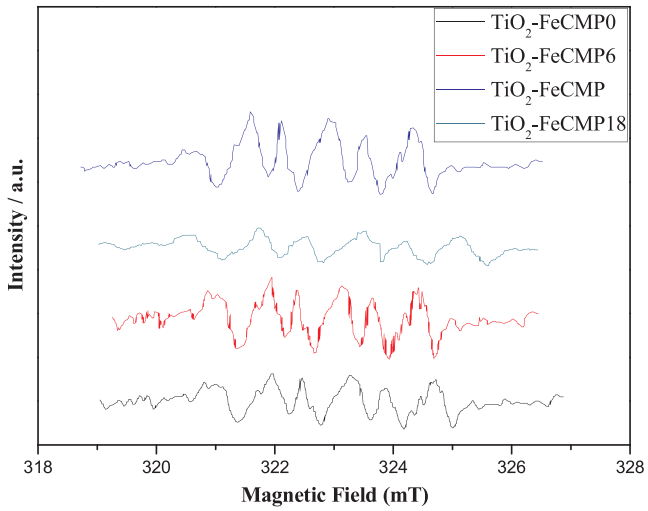

Fig. 9. ESR spectra of TiO_2-FeCMP series under visible light irradiation.

(Figs. S15a and S15c). TiO_2-FeCMP showed the highest diffusion current among the series (Fig S14), which was consistent with the degradation results (Fig. S11). As such, it seemed feasible that multi-electron ORR played a key role in the improvement of photocatalytic performance, and four-electron oxygen reduction process was better than two-electron oxygen reduction process.

To further confirm the relationship between multi-electron ORR and photocatalytic performance, the DMPO-$^{\cdot}CH_2OH$ spin adducts formed in the visible light irradiated methanol suspensions of TiO_2-FeCMP series in the absence of oxygen were detected by ESR spectroscopy (Fig. 9). The characteristic ESR sextet peaks of DMPO-$^{\cdot}CH_2OH$ spin adducts were found clearly under visible-light irradiation for TiO_2-FeCMP

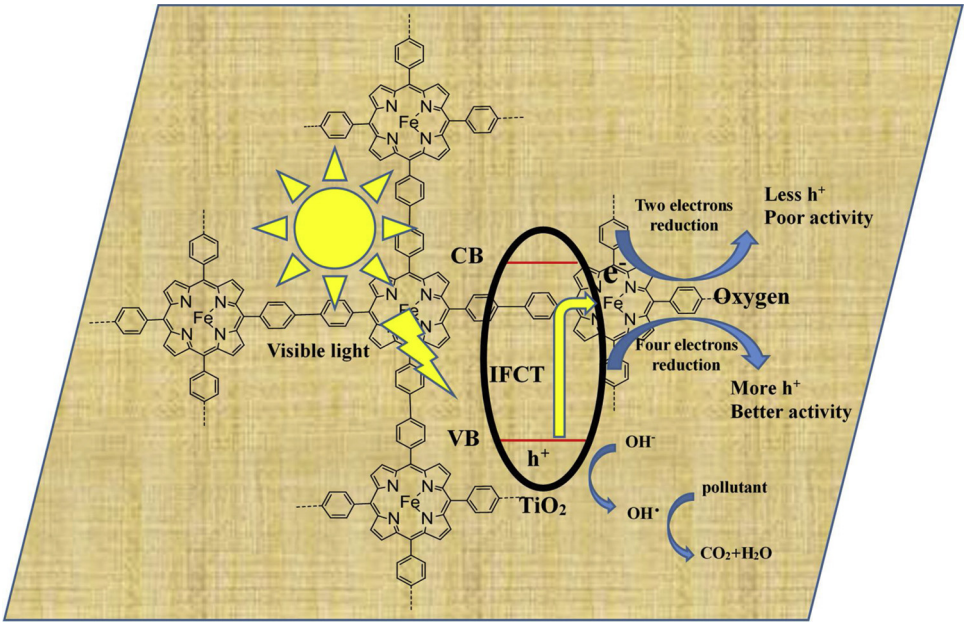

Fig. 10. Photocatalytic mechanism of TiO_2-FeCMP under visible light irradiation.

series, which was ascribed to the generation of photoinduced holes in the IFCT process. It could be found that the peaks intensity of TiO_2-FeCMP and TiO_2-FeCMP6 were higher than TiO_2-FeCMP0 and TiO_2-FeCMP18, which was consistent with the photocatalytic performance (Fig. S11), suggesting that four-electron oxygen reduction process might be better to accelerate the consumption of photoinduced electrons in the IFCT process than two-electron reduction, leaving more photoinduced holes in the valance band of TiO_2 for further degradation, resulting in better photocatalytic activity.

The photocatalytic mechanism was proposed (Fig. 10). IFCT effect from the valance band of TiO_2 to the Fe (III) in the FeCMP was triggered in the TiO_2-FeCMP compound under visible light irradiation. Meanwhile, the excited electrons were consumed on FeCMP through multi-electron ORR, which promoted IFCT effect. Further, it was revealed that four-electron oxygen reduction process was better to accelerate the consumption of photoinduced electrons than two-electron reduction in the IFCT process, leaving more photoinduced holes in the valance band of TiO_2 for further degradation, resulting in better photocatalytic activity. Moreover, TiO_2-FeCMP showed great chemical stability after several times recycle (Fig. S16).

4. Conclusion

In conclusion, FeP based CMPs were assembled on the surface of TiO_2 microspheres to prepare an efficient visible-light-driven photocatalyst, where IFCT process was supposed to be the primary reason for the enhancement of photocatalytic performance under visible light irradiation. In addition, the relationship between IFCT effect and multi-electron ORR was claimed, and it was believable that four-electron oxygen reduction process was better able to accelerate the generation of photoinduced holes in the IFCT process, resulting in higher photocatalytic activity.

Conflict of interest

The authors declare no competing financial interest.

Acknowledgement

The present work has been supported by the “National Natural Science Foundation of China (Grant 51573058)”.

Appendix A. Supplementary data

Supplementary material related to this article can be found, in the online version, at doi:https://doi.org/10.1016/j.apcatb.2019.03.075.

References

[1] R. Asahi, T. Morikawa, T. Ohwaki, K. Aoki, Y. Taga, Science 293 (2001) 269–271.
[2] J. Xu, Y. Chen, Z. Dong, Q. Wang, Y. Situ, H. Huang, J. Mater. Sci. 53 (2018) 12770–12780.
[3] T. Phongamwong, W. Donphai, P. Prasitchoke, C. Rameshan, N. Barrabés, W. Klysubun, G. Rupprechter, M. Chareonpanich, Appl. Catal. B 207 (2017) 326–334.
[4] J. Spadavecchia, C. Methivier, J. Landoulsi, C.M. Pradier, Chemphyschem 14 (2013) 2462–2469.
[5] J. Xu, Z. Dong, T. Hu, Y. Peng, Y. Situ, H. Huang, J. Alloys. Compd. 781 (2019) 140–148.
[6] Y. Chen, W. Huang, D. He, Y. Situ, H. Huang, ACS Appl. Mater. Interfaces 6 (2014) 14405–14414.
[7] X. Qiu, M. Miyauchi, K. Sunada, M. Minoshima, M. Liu, Y. Lu, D. Li, Y. Shimodaira, Y. Hosogi, Y. Kuroda, K. Hashimoto, ACS Nano 6 (2012) 1609–1618.
[8] M. Liu, X. Qiu, M. Miyauchi, K. Hashimoto, Chem. Mater. 23 (2011) 5282–5286.
[9] H. Irie, K. Kamiya, T. Shibanuma, S. Miura, D.A. Tryk, T. Yokoyama, K. Hashimoto, J. Phys. Chem. C 113 (2009) 10761–10766.
[10] M. Liu, X. Qiu, M. Miyauchi, K. Hashimoto, J. Am. Chem. Soc. 135 (2013) 10064–10072.
[11] W. Sun, H. Zhang, J. Lin, J. Phys. Chem. C 118 (2014) 17626–17632.
[12] M. Neamţu, C. Nădejde, V.D. Hodoroaba, R.J. Schneider, U. Panne, Appl. Catal. B 232 (2018) 553–561.
[13] M. Wei, J. Wan, Z. Hu, Z. Peng, B. Wang, H. Wang, Appl. Surf. Sci. 391 (2017) 267–274.
[14] K.S. Min, R.S. Kumar, J.H. Lee, K.S. Kim, S.G. Lee, Y.-A. Son, Dye. Pigment. 160 (2019) 37–47.
[15] X.L. Xin Zhao, Mimi Yu, Chen Wang, Jun Li, Dye. Pigment. 13 (2017) 648–656.
[16] G. Mele, R. Del Sole, G. Vasapollo, E. García-López, L. Palmisano, M. Schiavello, J. Catal. 217 (2003) 334–342.
[17] D.H. Lee, S. Kim, M.Y. Hyun, J.-Y. Hong, S. Huh, C. Kim, S.J. Lee, Chem. Commun. 48 (2012) 5512–5514.
[18] A. Nagai, X. Chen, X. Feng, X. Ding, Z. Guo, D. Jiang, Angew. Chemie Int. Ed. 52 (2013) 3770–3774.
[19] Z.S. Wu, L. Chen, J. Liu, K. Parvez, H. Liang, J. Shu, H. Sachdev, R. Graf, X. Feng, K. Mullen, Adv. Mater. 26 (2014) 1450–1455.
[20] J.R. Stromberg, J.D. Wnuk, R.A.F. Pinlac, G.J. Meyer, Nano Lett. 6 (2006) 1284–1286.
[21] L. Wang, Y. She, R. Zhong, H. Ji, Y. Zhang, X. Song, Org. Process Res. Dev. 10 (2006) 757–761.
[22] F.S. Hasobe T, P.V. Kamat, J. Am. Chem. Soc. 127 (2005) 11884–11885.
[23] S. Okada, H. Segawa, J. Am. Chem. Soc. 125 (2003) 2792–2796.
[24] M. Kandaz, A.T. Bilgiçli, A. Altındal, Synth. Met. 160 (2010) 52–60.
[25] M. Miyauchi, H. Irie, M. Liu, X. Qiu, H. Yu, K. Sunada, K. Hashimoto, J. Phys. Chem. Lett. 7 (2016) 75–84.
[26] S. Brüller, H.-W. Liang, U.I. Kramm, J.W. Krumpfer, X. Feng, K. Müllen, J. Mater. Chem. A 3 (2015) 23799–23808.
[27] K. Müller, M. Richter, D. Friedrich, I. Paloumpa, U.I. Kramm, D. Schmeißer, Solid State Ion. 216 (2012) 78–82.
[28] R. Kumar, S. Govindarajan, R.K. Siri Kiran Janardhana, T.N. Rao, S.V. Joshi, S. Anandan, ACS Appl. Mater. Interfaces (2016) 27642–27653.